J. Fluid Mech. (1990), *vol.* 219, *pp.* 241–271
Printed in Great Britain

Interaction of a deformable bubble with a rigid wall at moderate Reynolds numbers

By PETER J. SHOPOV†, PETER D. MINEV, IVAN B. BAZHLEKOV AND ZAPRYAN D. ZAPRYANOV

Institute of Mechanics and Biomechanics, Bulgarian Academy of Sciences, P.O. Box 373, Sofia 1090, Bulgaria

(Received 2 October 1987 and in revised form 13 March 1990)

The unsteady viscous flow induced by a deformable gas bubble approaching or receding away from a rigid boundary is investigated for moderate Reynolds numbers. The full Navier–Stokes equations were solved by means of a finite-element method. The bubble is driven by the buoyancy force. The performance of the numerical scheme is displayed for two different configurations of the flow: the bubble moves (i) in the half-space bounded by a rigid plate; (ii) in a spherical container filled with viscous fluid. Results are obtained for the evolution of the flow pattern and bubble shape for a number of values of Reynolds and Eötvös numbers: $2.2 \times 10^{-3} < \mathscr{R} < 60$, $1 < \mathscr{E} < 360$. The influence of specific values of $\mathscr{R}$, $\mathscr{E}$ and wall curvature on the shape of the deformable interface is thoroughly investigated. Several physical effects are included in our theory: dimpling and film formation; appearance of a concavity at the rear of the bubble for intermediate Reynolds numbers; and elongation of the bubble receding from the wall. Where possible comparisons are carried out with other experimental or numerical investigations. The good agreement achieved confirms the reliability of the numerical technique developed, of the results presented and the conclusions.

1. Introduction

The practical importance of studying bubble and drop motions is due to their common occurrence in many industrial and biological systems as well as in a number of technological processes (e.g. gas–liquid extraction, fluidized beds, flotation, fermentation, sedimentation, etc.). For instance, the motion of a bubble towards a rigid wall is connected with film drainage problems, being the initial stage of the latter. It is particularly important to investigate the motion of a deformable particle in a spherical container, which is an essential part of the multiple-drops theory and a prerequisite for creating models for the process of fabricating high-compression confinement fusion (ICF) targets, see Mok & Kim (1987). These problems represent only a few of the reasons stimulating an increasing amount of basic and applied studies in this research field.

There is a large number of theoretical studies dealing with bubbles and drops in inviscid flows. Such studies usually take the following general approach. The fluid is supposed to be incompressible and irrotational which imply that the flow is a potential one. The dynamics of the liquid is described by the simple Laplace equation. This is an essential simplification of the problem. Using potential theory

† Present address: Institute of Mathematics, Bulgarian Academy of Sciences, acad. G. Bontchev str., bl. 8, 1113 Sofia, PO Box 373, Bulgaria.

we can derive nonlinear equations for the velocity potential at the deformable interface for the motion of the latter. In this way Miksis, Vanden-Broeck & Keller (1982) studied the steady rise of a bubble in unbounded liquid and accounted for the surface-tension effect. A system of integro-differential equations was derived, including the normal component of the free-surface force balance, and treated numerically. The assumption of inviscid external flow used by these authors leads to violation of the tangential component of the boundary condition and reduces the practical importance of their results. That paper also contains a review of the previous works on the subject.

The transient behaviour of a cavitation bubble in inviscid liquid near a rigid or free surface was studied by Blake, Taib & Doherty (1986, 1987). In such problems the bubble volume changes with time and the evolution of the process is the subject of main interest here. The problem is modelled via a system of integral equations and solved by the boundary-integral method. A Lagrangian description of the bubble surface is employed. These techniques allow the problem to be studied in detail and produce many interesting bubble shapes. The influence of gravity is also considered. An essential advance achieved by Blake *et al.* is their treating of the unsteadiness and the influence of a rigid or a free interface on the cavitation process. However, the role of surface tension has not been studied by them.

A similar but more sophisticated numerical method was developed by Dommermuth & Yue (1987) for the same class of problems. They used a regridding algorithm to remove the instabilities. This algorithm allows longer time simulations than previous ones. They studied numerically the same problem as Blake *et al.* (1987) and reported very good agreement with the experimental measurements. Two wave–body interaction problems were also treated. The results confirmed the universality and good accuracy of the method.

It seems that numerical boundary-integral methods are a very promising tool for modelling the dynamics of deformable particles in inviscid flows. But they are based on the Bernoulli equation for the ambient liquid and are not applicable to viscous fluids.

Theoretical studies of the motion of deformable particles in a viscous liquid have been less numerous but still a number of stationary limiting cases have been treated in the literature. These are low- or moderate-Reynolds-number flows past a bubble or a drop with or without acknowledging the deformability of the particle surface.

The steady rise of an undeformable gas bubble in incompressible viscous fluid with very high Reynolds number ($\mathscr{R}$) and very low Weber number ($\mathscr{W}$) was investigated by Levich (1949). The bubble is assumed to be spherical and the existence of thin viscous boundary layers at both sides of the interface is supposed. Using boundary-layer theory, Moore (1963) and Chao (1969) improved Levich's results for bubbles and drops, respectively. El Sawi (1974) extended Moore's analysis and studied the interaction between the boundary layer and the bubble shape.

The limiting case of very small Reynolds numbers is often treated as well. Under this restriction Taylor & Acrivos (1964) developed an asymptotic expansion for the deformation of a drop falling through another unbounded liquid. They proved that under the Stokes approximation the drop will remain spherical for any Weber number.

Perhaps the first systematic numerical computations of steady viscous flow past a fixed spherical gas bubble were reported for $0.1 \leqslant \mathscr{R} \leqslant 200$ by Bradston & Keller (1975). They obtained good agreement for the drag coefficient with Moore's (1963) asymptotic theory for $\mathscr{R} = 40$ and with the small-Reynolds-number asymptotic

theory for $\mathscr{R} < 1$. The method of series truncation is used to reduce the problem to a nonlinear two-point boundary problem, solved by a finite-difference procedure. An essential restriction used in this work is that the bubble is assumed to be spherical.

Recently a couple of studies have appeared treating the more difficult case of intermediate Reynolds numbers and comparatively high Weber numbers. In such problems full steady Navier–Stokes equations have to be treated to describe the dynamics of the ambient fluid. Ryskin & Leal (1984) used a finite-difference method combined with numerical grid generation and obtained results for the steady rise of a deformable gas bubble in unbounded liquid for $1 < \mathscr{R} < 200$ and $\mathscr{W} < 20$. Christov & Volkov (1985) investigated the same problem in approximately the same ranges of the parameters but using a simple scaling of the independent coordinate in the frame of the finite-difference splitting technique. Both cited papers consider only a stationary single bubble in unbounded liquid. The same problem was studied experimentally by Bhaga & Weber (1981) and Hnat & Buckmaster (1976). They provided data widely used for the verification of the theories.

The interaction of a deformable particle with an interface is less widely studied. Basically, such problems are transient and also the domain occupied by the liquid changes, not only owing to the interface deformability but also to the particle motion. To overcome these difficulties in the limiting case of low Reynolds numbers the quasi-steady approach was employed. In this way, under the additional assumption of the law deformability of the interface, the slow motion of a drop with fixed velocity towards a plate was considered by Chervenivanova & Zapryanov (1985). First they solved analytically Stokes equations around an undeformed particle and then determined the shape of the interface satisfying the normal stress balance over it. But the resulting flow does not correspond to the shape evaluated and hence the results are legitimate only for the case of small deformations.

In those works the transient effects are not taken into account. Such effects are particularly important when a particle is started from rest or when it approaches an interface. Some film-thinning problems could be considered as limiting cases of the interaction of a bubble or a drop with an interface for large times and small distances between the particle and the wall. The usage of the full unsteady Navier–Stokes equations with free boundary conditions seems to be relevant for the first stage of the process when the standard film-theory conditions are not satisfied. So the interaction of a deformable particle with an interface is connected with film problems.

A theoretical approach to the film-thinning problem was proposed by Reed, Leidi & Hartland (1980). They proposed a mathematical model for the final (drainage) stage of the approach of a drop to a horizontal plate, assuming that the standard thin-film-theory assumptions are satisfied and that the initial thickness of the film is constant. This model is not applicable, however, for relatively large distances between the particle and the plate; here the deformable particle–interface interaction model could be used. The results of experiments contained in Reed *et al.* and in the works of Hartland (1967) and Mackay & Masson (1963) could be used for qualitative and quantitative verification of such theories for the inception of film formation.

Another class of transient problems is the motion of a deformable drop in confined fluid. The dynamics of a bubble in a container is an example of such situation. The case of a spherical container has been studied theoretically by several authors. Mok & Kim (1987) considered this problem with the approximation of low Reynolds and low Prandtl numbers, assuming that the bubble is spherical, concentric with the container and moving with its terminal velocity. They also took into account the vertical temperature gradient and the gravity force. The method employed is an

analytical one and is based on series expansions in terms of Gegenbauer polynomials for the velocity and Legendre polynomials for the temperature. A slightly deformable bubble moving with a fixed velocity in a spherical container of liquid was considered by Chervenivanova & Zapryanov (1987) with a low-Reynolds-number approximation (see also references therein). They employed the same method as in their work previously mentioned. In these works the influence of the ratio of the bubble and the container diameters (it represents the curvature of the wall too) and the finite size of the container were considered. Brunn & Roden (1985) obtained an approximation, first-order in Reynolds number, for a similar problem in connection with type-A multiple drops, once again under the low-Reynolds-number assumption. In this study the surface force balance conditions are imposed on an undeformable spherical fluid interface rather than the non-slip conditions at the rigid container wall.

As far as we know the hydrodynamical interaction of deformable particles with a flat or spherical rigid wall has not yet been investigated for intermediate Reynolds and Weber numbers. This is an interesting nonlinear physical problem of fundamental importance whose solution is crucial for providing the film-thinning theory with more consistent initial conditions and for defining the time moment after which this theory can be applied.

In this paper we develop a numerical technique for evaluating the non-steady hydrodynamical interaction of a bubble with a rigid wall. We consider the following two basic problems: (i) the motion of a bubble near a plane rigid interface; (ii) the motion of a bubble in a spherical rigid container.

In our investigations the driving force is the buoyancy. At the initial moment the bubble is assumed to be at rest, its shape spherical and the ambient liquid quiescent. The fluid in the bubble is assumed to be ideal, incompressible and at constant pressure. All nonlinear terms are retained and large deformations of the interface are allowed. On the bubble interface the surface tension is taken into account.

Our theory could also be applied to drops, if the viscosity of the fluid inside is negligible and the motion of the fluid in the drop can be ignored.

We obtain the bubble shape, velocity and flow pattern around it as functions of time. The temporal deformation of the bubble with time and the distance between the bubble and the wall are also calculated. The influence of inertial and viscous forces (represented by the Reynolds number), surface-tension and gravity forces (represented by the Eötvös number, E), the dimensionless starting distance from the wall and the wall curvature (represented by its radius) are studied.

Various physical effects are observed in our calculations: dimpling and film formation; appearance of a concavity in the rear part of the bubble for intermediate Reynolds numbers; and elongation of a bubble receding from a wall. Two new effects are also studied. The first is the formation of a slight dimpling ring, instead of the usual dimple, on the spherical film between the bubble surface and the container. The second is the existence of a surface wave at the rear portion of the bubble when the latter recedes from the container wall. This effect is observed only for relatively large Reynolds and intermediate Eötvös numbers.

Our theory yields some information about the inception of film and dimple formation. However, it cannot be applied directly to the study of thin-film problems, because in this case the efficiency of the numerical method is too low. Our results just give more precise initial conditions for film-drainage theories.

Preliminary notes about the results presented are published in Minev, Shopov & Zapryanov (1988), Bazhlekov, Shopov & Zapryanov (1989) and Shopov *et al.* (1989*b*).

In the next section we describe the mathematical model. This is followed by some information about the numerical method used. Its complete description will be published separately in Shopov, Minev & Bazhlekov (1990). In the following section (§4) some test problems and comparisons to theoretical and experimental works are presented to demonstrate the accuracy of the numerical modelling. Section 5 begins with an overall description of the numerical experiments. The results for the temporal evolution of the bubble shape, velocity field and instantaneous streamlines are shown and interpreted. Parametrical investigations are also presented. The final section summarizes the main conclusions and identifies some fields of future investigations.

2. Formulation of the problems and mathematical model

We consider the following two problems:

(i) the rise of a deformable gas bubble towards or away from a plane rigid wall in unbounded liquid at moderate Reynolds numbers;

(ii) the motion of a gas bubble in a spherical container filled with viscous liquid for moderate values of the Reynolds number.

In both problems the bubble and the liquid are initially motionless and the motion is set up by the buoyancy.

The geometry of the problems is illustrated on figure 1. Note that generally speaking the first problem could be considered as a limiting case of the second one when the radius of the container tends to infinity.

The fluid in the bubble is assumed to be incompressible with density $\rho_0 = 0$, viscosity $\mu_0 = 0$, and the pressure inside, $p_0(t)$, does not depend on the spatial coordinates. This assumption is valid for an ideal gas if the pressure and temperature differences in the ambient liquid are not too large. Physically this means that the dynamics of the fluid in the bubble is ignored. The ambient liquid is homogenous, incompressible and Newtonian, with constant physical properties; dynamic viscosity μ and density ρ. The coefficient of surface tension of the interface between the gas and the liquid is σ. The pressure at infinity is assumed to be constant. Initially the bubble and ambient liquid are at rest and the bubble is spherical.

Our model can also be applied to the more general case when the density of the fluid in the drop is $\rho = \text{const}$. Then the pressure inside the drop is

$$p_i = p_0 + \rho_0 g(z_0 - z), \quad z_0 = z(B). \tag{2.1}$$

This assumption is valid for an ideal liquid if the deformation of the interface is sufficiently slow. Thus, a drop with negligible viscosity can be also treated in this manner.

The diameter $2l$ of an equivalent spherical bubble (with the same volume) is chosen to be the reference length and the so-called Stokes terminal velocity U_0 is chosen to be the characteristic velocity:

$$l = \left(\frac{3}{4\pi} V\right)^{\frac{1}{3}}, \quad U_0 = \tfrac{2}{9}\rho g l^2 \lambda/\mu, \tag{2.2}$$

where V is the volume of the bubble, $\lambda = (\rho - \rho_0)/\rho$ is the ratio of the difference in the densities of the liquid and the gas to the density of the liquid, g is the gravitational acceleration.

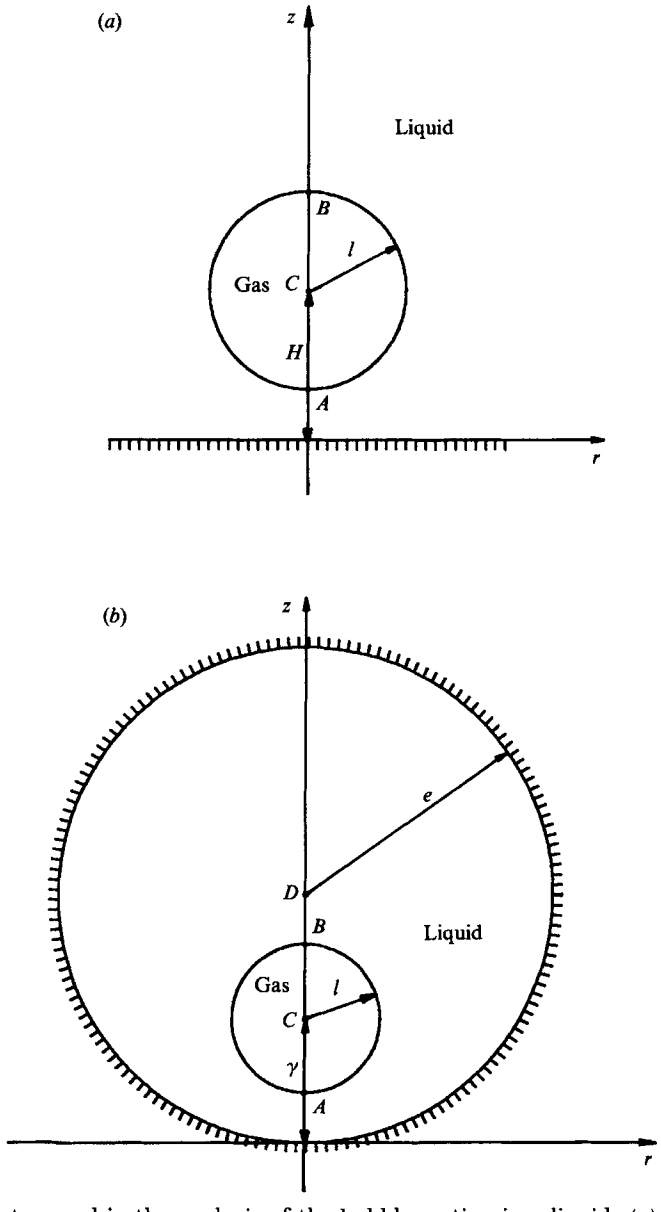

FIGURE 1. Geometry used in the analysis of the bubble motion in a liquid: (*a*) near a rigid interface; (*b*) in a spherical container.

The numerical results are presented in terms of Reynolds and Eötvös numbers:

$$\mathscr{R} = \rho(2l)U_0/\mu, \quad \mathscr{E} = g(2l)^2\rho\lambda/\sigma. \tag{2.3}$$

Thus $\mathscr{R}$ determines the relative importance of the inertial to the viscous force and $\mathscr{E}$ of the gravitation force to surface tension.

The commonly used Morton, Weber and Froude numbers

$$\mathscr{M} = g\mu^4\lambda/\rho\sigma^3, \quad \mathscr{W} = l\rho U_0^2/\sigma, \quad \mathscr{F} = U_0^2/(gl\lambda), \tag{2.4}$$

are expressed through $\mathscr{R}$ and $\mathscr{E}$ for this choice of reference velocity:

$$\mathscr{M} = 18^{-2}\mathscr{E}^3/\mathscr{R}^2, \quad \mathscr{W} = 18^{-1}\mathscr{R}\mathscr{E}, \quad \mathscr{F} = 18^{-1}\mathscr{R}. \tag{2.5}$$

The number 18 appears due to the coefficient $\frac{2}{9}$ in the reference Stokes velocity, cf. (2.2).

Respectively, the capillary number and the drag coefficient read

$$\mathscr{C} = U_0\mu/\sigma = \frac{1}{18}\mathscr{E}, \quad C_D = \tfrac{4}{3}glU_0^{-2} = 24/(\lambda\mathscr{R}). \tag{2.6}$$

The problem depends on two geometrical parameters:

$$\gamma = H/2l, \quad e = 2R/2l, \tag{2.7}$$

where H is the initial distance from the bubble centre to the rigid boundary, R is the radius of the container (for Problem (i) $R = \infty$). The first, γ, represents the dimensionless starting distance and determines the initial location of the bubble. The second one expresses the ratio of the diameter of the container to the initial diameter of the bubble and determines the relative importance of the curvature of the wall.

Provided that the plate is horizontal and the Reynolds number is not too high there is no asymmetry and the flow is two-dimensional. So one can employ the axisymmetric Navier–Stokes equations:

$$\mathrm{D}\boldsymbol{v}/\mathrm{D}t = -\nabla\bar{p} + \nabla\cdot\boldsymbol{T} + \boldsymbol{F}, \tag{2.8}$$

$$\nabla\cdot\boldsymbol{v} = 0, \tag{2.9}$$

$$\boldsymbol{T} = (1/R)\boldsymbol{D}; \quad \boldsymbol{D} = 0.5(\nabla\boldsymbol{v} + \nabla\boldsymbol{v}^{\mathrm{T}}) \tag{2.10}$$

where $\boldsymbol{v} = (v_r, v_z) = (U, V)$, $\boldsymbol{x} = (r, z)$, $\boldsymbol{F} = (0, -1/\mathscr{F})$, $\bar{p} = p - \rho_0 g(z_0 - z)$, and p is the pressure.

The standard no-slip conditions are imposed on the rigid wall and at infinity:

$$\boldsymbol{v} = 0. \tag{2.11}$$

The symmetry conditions with respect to the line $r = 0$ have the form

$$v_r(r, z) = -v_r(-r, z), \quad v_z(r, z) = v_z(-r, z), \quad p(r, z) = p(-r, z). \tag{2.12}$$

We need these conditions to close the boundary-value problem in the half-domain $r > 0$.

The standard boundary condition at the free surface expresses the balance of the normal stresses:

$$\boldsymbol{T}\cdot\boldsymbol{n} + (p_0 - \bar{p})\boldsymbol{n} - \mathscr{W}^{-1}(1/R_1 + 1/R_2)\boldsymbol{n} = 0, \tag{2.13}$$

where $\boldsymbol{n}$ is unit outward normal to the free surface; R_1 and R_2 are the principle radii of curvature of the interface (see e.g. Keunings (1986) and references therein).

The free surface satisfies the kinematic condition

$$\mathrm{D}S/\mathrm{D}t = \partial S/\partial t + \boldsymbol{v}\cdot\nabla S = 0, \tag{2.14}$$

where $S(r, z, t) = 0$ is the equation of the free surface.

The initial conditions for a quiescent liquid and a spherical bubble at rest (see figures 1 and 2) are

$$\boldsymbol{v}|_{t=0} = 0, S|_{t=0} = S_0. \tag{2.15}$$

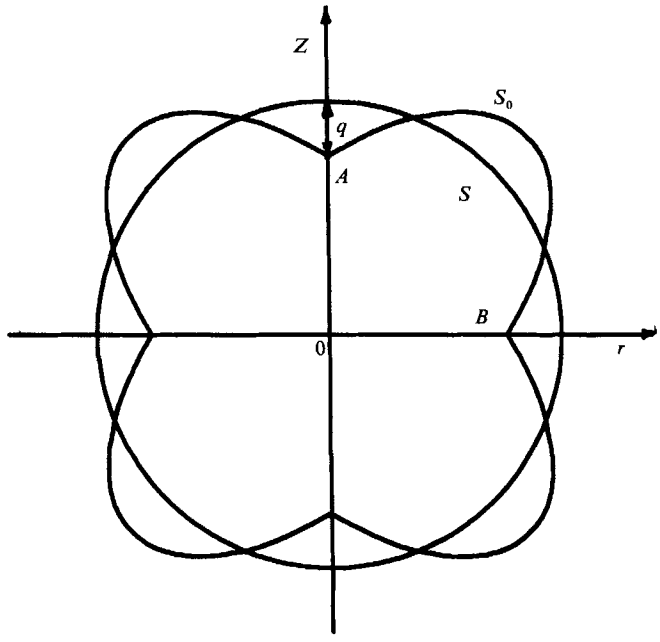

FIGURE 2. Deformed initial surface S_0 of the bubble and its final stable shape S.

3. Numerical method

At present there exists a variety of numerical methods for solving unsteady Navier–Stokes equations when free boundaries are present. They can be divided into two classes: (i) finite-difference methods in (ω, ψ) variables – Christov & Volkov (1985), Kang & Leal (1987), Shokoohi & Elrod (1987); (ii) finite-element methods (FEM) in primitive variables (velocity and pressure) (see Keunings 1986 and references therein). Both approaches have their own advantages and disadvantages.

FEM algorithms are very natural and have proven their good performance in solving Navier–Stokes equations even in the case of transition to a turbulent regime (Fortin, Fortin & Gervais 1987; Jackson 1987). Transient free-surface entrainment and circulation problems (Frederiksen & Watts 1981) as well as jet stability problems (Keunings 1986) can also be treated by FEM. The cited methods are of Lagrangian–Eulerian type.

Our numerical method is conceptually akin to these methods. The general idea is quite an old one (see Connor & Brebbia 1977 and references therein) and is a type of Lagrangian approach.

Here we shall not describe the algorithm in detail (see Shopov 1985, 1988; Shopov & Minev 1986). The complete account of the development of the technique will be published by Shopov *et al.* (1990). Here we shall just point out its main differences from the techniques of Frederiksen & Watts (1981) and Keunings (1986).

In the present paper the Lagrangian approach is used, because it has significantly lower numerical diffusion errors than Eulerian and Lagrangian–Eulerian ones – see Cloutman (1987) and references therein. The mesh cells represent finite volumes of the liquid which move with the flow and deform until they stretch intolerably, when the grid is redefined. Usually only a couple of grid redefinitions appear to be

necessary, i.e. the computations are almost Lagrangian. Our method possesses all the standard advantages of the Lagrangian method: (i) natural tracking of discrete fluid volumes and the free-surface boundary; (ii) a clear physical meaning of the discrete mathematical model; (iii) natural and simplified treatment of the convection.

Our algorithm is provided with a general procedure for grid redefinition, which can even change the number of finite elements as well as the mesh topology (Shopov, Minev & Bazhlekov 1989*a*). The moment when regridding is needed is determined automatically. The new mesh is introduced by means of a standard grid generator (Shopov (1985). The velocity field is defined in the whole region by its values on the old mesh and hence at the new nodes too. Then the velocity at new nodes is evaluated. The spatial positions of the mesh points are not predetermined by the position of the free surface, which allows us to change the density of the grid in different regions during the computations.

The integration of the kinematic condition (2.7) is accurately performed without introducing additional unknowns for the position of the deformable interface. So we can use a smaller number of unknowns than is usually done in an FEM. A predictor-corrector method is used to ensure accuracy when calculating the position of the free surface.

Here we should mention that in the present work we employ a more sophisticated approximation (Shopov & Minev 1986) of the free-surface and surface-tension operator than the standard one (see e.g. Keunings 1986 and references therein). It is introduced because the classical one does not preserve the spherical shape of a bubble at rest in unbounded liquid in weightlessness. It also provides the means for direct control of the smoothness of the interface.

We incorporate in our numerical scheme an optional spline procedure for filtering the error in the computed values of the velocity on the free boundary. It should be stressed here that the filtering is not a necessary condition for the stability of the algorithm proposed and numerical results in some cases have been obtained without its use. What makes the difference, however, is that the convergence is radically improved with the filtering and as a result the required computational time is reduced (Shopov *et al.* 1989*a*).

Based on the standard idea of predictions–corrections (see e.g. Gresho, Lee & Sani 1980), Shopov (1988) developed a practical criterion for automatic adjustment of the time spacing in order to optimize the required computational time and this is used in the present work. Another important feature of the algorithm is the automatic control on the accuracy of the free-surface computation, see also §5.1.

Let us note that the FEM approximation proposed here reduces to a positive definite system of linear equations (Shopov 1984). In this instance our technique is similar to a divergence-free one – see e.g. Cuvelier, Segal & Steenhoven (1986).

We use isoparametric finite elements of second-order accuracy with biquadratic continuous velocity and linear discontinuous pressure. These finite elements possesses excellent properties for incompressible flows (Fortin *et al.* 1987; Jackson 1987; Cliffe & Lever 1986) and seem to be the best choice for the axisymmetric case, when the non-conforming triangles do not satisfy the path test.

We do not claim, of course, that all of the above-described differences are necessarily advantages in each specific case. Only a detailed comparison between the methods can answer the question which of them is better, for a specific problem and on a particular computer: different numerical methods possess their own advantages for the class of problems for which they are constructed. In this instance, our

technique is particularly suited for numerical solution of free-surface fluid problems.

Based on it a rather general code, NEFIS, is developed, by which all computations presented are done.

As usual, the accuracy of the numerical method and the code have been verified on various test problems. Several comparisons related to undeformable and deformable particles are presented in the next section, which confirm the good accuracy of the method. Other examples are presented in Shopov *et al.* (1990).

It is difficult to assess *a priori* the final accuracy of the numerical methods. It depends not only on the quality and the conservation properties of the method but also on the properties of the unknown solution, the density of the grid and the maximal time-integration step. In our case the influence of these parameters is partially included in the gross measure of the total accuracy of the free-surface computation ϵ (here $\epsilon = 2.5\%$ or less, see §5.1), which gives an idea of the total precision of the results. As always with numerical methods, comparisons with other analytical, numerical and experimental solutions as well as information from the own numerical experiments and the self-consistency of the data gives a feeling for the real accuracy of the results. Existing experience of similar problems also plays an important role.

On the grounds of these criteria we assess the accuracy of results presented to be not worse than 5%. In many cases the accuracy is much better. In our opinion the qualitative behaviour of the predicted shapes is always very reliable, even if the observed effects are quantitatively smaller than the upper error limit. This is connected with the good conservation properties of this method (Shopov 1989) and with the clear physical meaning of the discrete model. The only assumptions used are the finite-element approximation of small liquid volumes and discrete time.

With the increase of the usage of numerical methods in free-surface fluid dynamics the task of establishing a set of standard test problems arises. This seems to be more or less settled only for laminar flow in fixed-domain, steady, simply connected cases, related to the investigations of a great number of authors – see e.g. Thomasset (1981) and Pirronneau (1984) and the references therein.

In this connection perhaps the steady motion of a deformable particle under buoyancy could be proposed as a standard test for the stationary case. For the unsteady case, in unbounded liquid, it could be the relaxation of the initially disturbed bubble (see §4), the deformation of a bubble in straining flow or under gravity and antigravity (see Kang & Leal 1987 and §4).

4. Test and comparisons

All numerical experiments are performed employing standard isoparametric 9-node velocity, linear discontinuous pressure finite elements, see e.g. Cuvelier *et al.* (1986), Fortin *et al.* (1987) and figure 4.

4.1. *Slow motion of a rigid sphere*

Consider the classical problem – slow motion of a rigid sphere with constant velocity in infinite viscous fluid – see Happel & Brenner (1965). It is reduced to the solution of the steady Stokes equations in fixed domain.

The problem is solved on several meshes with different numbers of nodes. Here we shall give only the result for a rather coarse mesh with four isoparametric finite elements, non-uniform in the radial direction in the ratio 1:4 and uniform in the other direction. Infinity is placed at 5 radii from the sphere. The problem is treated

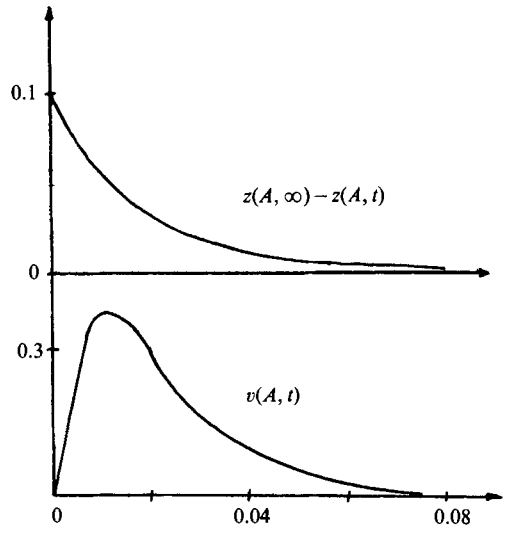

FIGURE 3. Numerical solution for initially disturbed bubble; $\mathscr{R} = 1$, $d = 0.1$.

in a quarter of the whole domain using two types of symmetry conditions. The maximum difference between the exact solution and numerical one in the mesh points is $|\boldsymbol{v}_{\text{exact}} - \boldsymbol{v}_{\text{numerical}}|_C = 0.0163$ for the velocity and for the stream functions $|\Psi_{\text{exact}} - \Psi_{\text{numerical}}|_C = 0.0027$, where $|\cdot|_C$ denotes the maximum norm. This accuracy is more than satisfactory for such a grid.

This simple problem is chosen as a test for the following reasons: (i) this exact solution of a flow past a particle is used in many physical applications; (ii) it gives an idea of what kind of meshes could be used; (iii) the time integration of the unsteady Navier–Stokes equations by Lagrangian-type methods is reduced to the solution of the Stokes equation at every time step.

There are many differences between this situation and the transient, free-surface case.

4.2. *Time relaxation of an initially disturbed bubble*

The part of the technique responsible for calculating the bubble shape is tested separately. For this purpose the gravity is 'switched off', taking $\mathscr{F}^{-1} = 0$. The stable shape of a unit bubble in quiescent, unbounded liquid is spherical – see Batchelor (1967). To test our algorithm on this well-known fact we disturb a spherical bubble shape such shown on figure 2 and follow its time evolution.

We choose as a characteristic length the radius of the undeformed spherical bubble l and as a characteristic time the surface-tension relaxation time $\mu l/\sigma$. So the fluid velocity is scaled by σ/μ and the pressure by σ/l.

The dimensionless amplitude of the disturbance is $q = 0.1$, and $\mathscr{R} = 1$. The maximum deviation from the stable shape is achieved at points A ('a hollow') and B ('a ditch'). We take a non-smooth initial shape to see how the non-physical edges and tops are smoothed down.

The temporal evolution of the deviation $z(A,\infty)-z(A,t)$ at the point A from its final stable position and the velocity $v(A,t)$ is shown on figure 3 for one particular case. This figure shows that the stable spherical shape is obtained after a time interval.

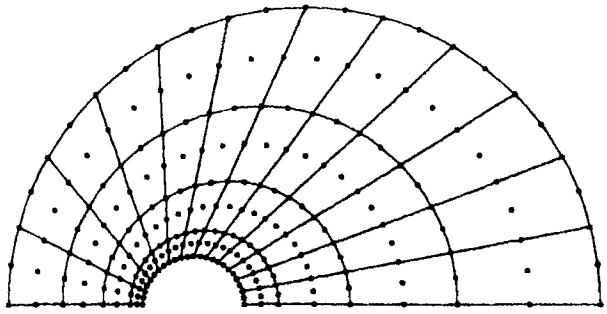

FIGURE 4. Example of a mesh used for modelling the steady rise of a bubble in unbounded liquid.

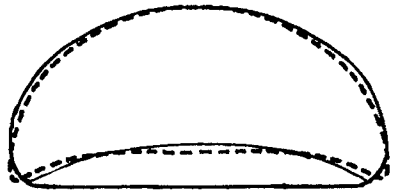

FIGURE 5. Comparison of numerical bubble shape with experiments (——) of Bhaga & Weber (1981) at $\mathscr{R} = 13.3$, $\mathscr{E} = 116$, $\mathscr{M} = 5.51$.

4.3. *Steady motion of a deformable bubble*

Next we do the following simple test. A spherical bubble at $\mathscr{R} = 0.0044$ and $\mathscr{E} = 0.2$; $\mathscr{W} = 0.00005$ moves owing to the buoyancy in unbounded liquid. The definition of the governing parameters is as described in §2. No deformation occurs, which is in agreement with the result of Taylor & Acrivos (1964) for $\mathscr{R} \ll 1$.

The steady motion of a deformable bubble in unbounded liquid has been studied experimentally by Bhaga & Weber (1981), Hnat & Buckmaster (1976) and numerically by Ryskin & Leal (1984), Christov & Volkov (1985). The stationary problem can be considered as a particular case of the transient one and hence the latter studies could be used for testing the numerical technique. Our method is developed especially for unsteady problems. A steady-state problem can be solved as the limit case ($t \sim \infty$) although this is an expensive procedure. Of course, special and more efficient variants of the method can be constructed for stationary problems.

In §4.3 the reference velocity and length are as chosen by Bhaga & Weber (1981), i.e. with respect to real terminal velocity and the volume-equivalent diameter. A model grid used for comparison is shown on figure 4. Regridding is applied when the particle moves far from the centre of the grid or the mesh becomes distorted. The usage of more grid points will yield better accuracy. The results presented show that even on such comparatively sparse meshes the accuracy is satisfactory.

We compare with two shapes experimentally obtained by Bhaga & Weber (1981). At $\mathscr{R} = 0.078$, $\mathscr{E} = 8.67$, $\mathscr{M} = 711$ the bubble is practically spherical. The numerical experiment shows deviation of less than 1% from the spherical shape. This is less than the accuracy of the experimental data. The comparison at large deformability and intermediate Reynolds number is shown on figure 5.

Bhaga & Weber (1981) have calculated the value of the separation angle as $\theta = 100°$ for the experiment depicted on figure 5. The value of θ in our computational

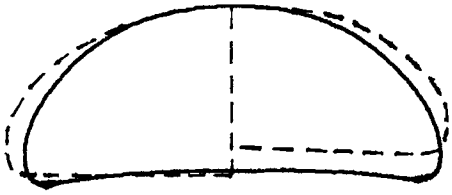

FIGURE 6. Comparison of our result at $\mathscr{R} = 19.4$, $\mathscr{W} = 15.3$ with the experiment (----) of Hnat & Buckmaster (1976) at $\mathscr{R} = 19.4$, $\mathscr{W} = 15.3$ (left-hand side) and with the theory (----) of Ryskin & Leal (1984) at $\mathscr{R} = 20$, $\mathscr{W} = 15$ (right-hand side).

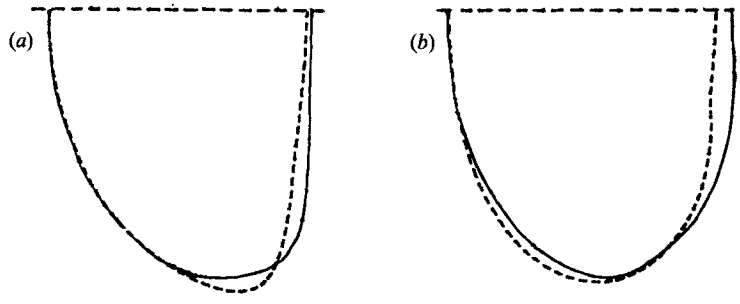

FIGURE 7. Comparison with the theory of Christov & Volkov (1985) (——) at (*a*) $\mathscr{R} = 20$, $\mathscr{W} = 7.64$, $\mathscr{M} = 6.83 \times 10^{-3}$; (*b*) $\mathscr{R} = 60$, $\mathscr{W} = 5.04$, $\mathscr{M} = 9.3 \times 10^{-6}$.

result is $\theta = 98°$. This also confirms the good agreement of our solution with the experimental data.

Ryskin & Leal (1984) compared their numerical solution for the steady rise of a bubble in viscous, unbounded liquid at $\mathscr{R} = 20$, $\mathscr{W} = 15$ with the experiment of Hnat & Buckmaster (1976) at $\mathscr{R} = 19.4$, $\mathscr{W} = 15.3$. Our result for the bubble shape is depicted on figure 6 for the same situation as in the experiment. The eventual concavity at the rear is invisible on the experimental photograph. It explains the difference with the numerical data.

Christov & Volkov (1985) have also studied this problem. The comparisons with their results at $\mathscr{R} = 20$, $\mathscr{W} = 7.64$, $\mathscr{M} = 6.83 \times 10^{-3}$ and $\mathscr{R} = 60$, $\mathscr{W} = 5.04$, $\mathscr{M} = 9.3 \times 10^{-6}$ are shown on figure 7(*a*, *b*).

Our numerical method is constructed specially for comparatively large Eötvös and Weber numbers. The result presented on figures 6 and 7 shows that it works better for large values of them than the numerical methods of Ryskin & Leal and Christov & Volkov. The large Reynolds numbers required small time steps and dense grids. So we restrict our comparisons to $\mathscr{R} = 60$. Cliffe & Lever (1986) considered $\mathscr{R} = 40$ as a typical value for intermediate Reynolds numbers.

These test problems and comparisons give us confidence in the accuracy of the interface shape, obtained by our numerical technique.

5. Numerical results

In this section we present results concerning the bubble shape, its deformation, velocity, instantaneous streamlines and the thickness of the liquid layer between the bubble and the wall that are predicted for the transient motion of a bubble in the presence of a rigid boundary.

Problems (i) and (ii) are solved for various values of the parameters. Two distinct

situations are considered: when the bubble approaches the wall and when it recedes away from the wall. The Reynolds number varies from 4×10^{-3} to 120, the Eötvös number from 1 to 360. The initial distances are taken from the interval $0.55 \leqslant d \leqslant 1$ ($\gamma = 0.5$ corresponds to the case when the bubble touches the wall), and the diameter of the container is allowed to vary from 2 up to ∞, the latter corresponding to the case of a planar wall. At the initial moment of time the bubble is at rest and the liquid is quiescent.

Bubble velocity $\boldsymbol{v}(C)$ is defined as the velocity at the bubble middle point C defined as $C = 0.5\,[z(A)+z(B)]$ and hence $\boldsymbol{v}(C) = 0.5\,[\boldsymbol{v}(A)+\boldsymbol{v}(B)]$. This definition as a rule serves reasonably well but differs from its usual meaning at the film stage, where more weight should be given to the velocity at the dimpling zone.

When the bubble approaches the rigid wall, a thin layer is formed, which can be considered as the first stage of film formation in the drainage process. In this case the velocity $\boldsymbol{v}(A) = \boldsymbol{v}(A,t)$ of the front point A of the bubble can be considered as a measure for the film thinning velocity, and the distance $d = d(t)$ from that point to the wall (see figure 1) as the dimensionless film thickness scaled with the volume-equivalent radius of the bubble. Since the thickness varies at different points we shall also use the notation $\mathscr{d}(x,t)$ (note that $d(t) = \mathscr{d}(0,t)$. In film-thinning theory the film thickness $\Delta(x,t)$ ($\Delta = \Delta(0,t)$) is scaled with the film length $r_f = r_f(t)$

$$\Delta(x,t) = \mathscr{d}(x,t)/r_f(t). \tag{5.1}$$

The last quantity is used only for large times when the film is already formed.

We have also studied the two different two-dimensional plane-parallel versions of problems (i) and (ii). The first is the problem of motion of a very long bubble near a plate, and the second its motion near a tube wall. These are models for quasi-two-dimensional experiments (see e.g. Reed *et al.* 1980). The agreement with those experiments is qualitatively good but we do not present the results since they go beyond the scope of the present work.

In the following subsections we consider several examples of bubble motion in the presence of a rigid interface and the influence of the governing parameters corresponding to four physical factors is studied.

The dimensionless height h and width w of the bubble are often measured in the experiments and it is instructive to compare our findings for those two quantities with the available data. We define $h = z(B)-z(A)$ (see figure 1). The aspect ratio w/h is considered as a measure of the average deformation.

5.1. *Overall description of the numerical experiments*

Triangulation is introduced for half of the real domain, see figures 1 and 8. We choose the maximal value of the time increment $\Delta t_{\max}$ from the interval $[0.1, 0.5]$ according to the requirements of the particular case under consideration. During the calculations the algorithm can automatically reduce the time increment in order to control the accuracy of calculation of the free surface or of its smoothness. The procedure for automatic time increment selection is that we require, at each time step, the following criterion to be satisfied:

$$|S^{\mathrm{p}} - S^{\mathrm{c}}|_{\mathrm{C}} < \epsilon\,\Delta t \tag{5.2}$$

(for the definition of $|\cdot|_{\mathrm{C}}$ see §4). In other words, the maximum of the difference between the predicted position of the free-boundary and its corrected position is to be less than a given accuracy ϵ multiplied by the time step. The definitions of S^{p} and S^{c} are given in Shopov (1988). The presence of Δt in (5.2) ensures that the error

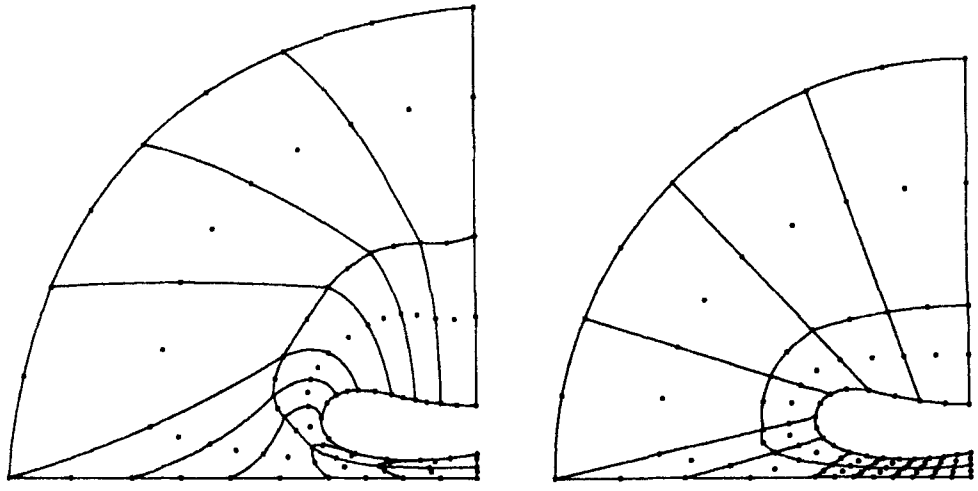

FIGURE 8. Example of a distorted mesh and a new one after regridding.

cannot increase. The gross measure ϵ for the accuracy is usually taken to be about 2.5% of the unit length. Satisfying (5.2) means that the specific error is essentially smaller for a particular time step.

The maximum value α of the angle between the normals at the junction points of the finite-element sides on the free boundary is used as the measure for the smoothness of the free surface. The difference approximation of the interface consists always of mesh nodes, because the numerical method is of Lagrangian type. Since the variable α is equal to zero for a real smooth surface we impose the following condition on it:

$$\alpha < \bar{\epsilon}. \tag{5.3}$$

This gives direct control of the smoothness of the free surface. The value $\bar{\epsilon}$ is measured in radians and is taken in our calculations not to exceed 0.22, i.e. about 10°. Such non-smoothness is so small that it is not visible even when the free surface is shown graphically.

If at a certain time stage the conditions (5.2) or (5.3) are not satisfied, Δt is reduced according to them and the time step is repeated. If (5.1) can be satisfied when, in place of ϵ, $\frac{1}{2}\epsilon$ is employed then Δt is increased (see Shopov 1988 for details). This procedure of time-increment management turned out to give values for Δt from 10^{-5} up to $\Delta t_{\max}$ (e.g. $\Delta t_{\max} = 0.2$) depending on the particular stage of evolution of the flow.

Remark 1. The time integration almost stops if Δt remains steadily low. Such situation occurs if the free surface becomes numerically unstable or an error exists in the program code or data. The numerical method automatically determines the moment when it can give good results.

So the exactness of the free-surface evaluation is carefully controlled. We have performed many numerical experiments with different numbers of finite elements or different choices of the time-integration step, including $\Delta t = \text{const}$. The results do not differ essentially, and we shall not present particular data on this here because several tests and comparisons are given in §4, which show the accuracy of the method.

In our method the mesh points represent the fluid particles and move over time. So the finite elements represent liquid volumes and also become distorted after a

time. The finite-element's shape is controlled automatically in the standard way for the FEM. The calculations stop when the value of the Jacobian for one finite element falls below 10^{-2} and grid redefinition is performed – see Shopov *et al.* (1989*a*). An example of such a situation is pictured on figure 8 for a coarse mesh.

Hence in general we can follow the shape evolution in time without any restrictions. But in practice one situation exists for which our method becomes very inefficient and time integration nearly stops – see *Remark 1*. This takes place when the film zone between the gas–liquid interface and the wall is formed and the motion of the bubble itself nearly stops. The velocities were of order 10^{-3}, so we expected that the pattern was connected with the choice of the reference velocity. We diminished the reference velocity (e.g. 10^{-3} times) and the velocities became of order one. But the time step was also decreased (measured with respect to the new reference time, of course, see §2) and the displacement remained unchanged. Hence in this way we have achieved nothing but an additional proof that the numerical results do not depend of the choice of the reference velocity.

This situation seems to us to be natural. From a mathematical point of view the error of the numerical method is proportional to the diameter $h_{\max}$ of the largest finite element in the computational domain – see e.g. Cuvelier *et al.* (1986). The thickness of the film zone is about two orders lower than the diameter of the bubble and hence much smaller than $h_{\max}$. Therefore the total error of the numerical method begins to be considerable in the film zone and spurious instability of the free surface takes place. We come to the situation described in *Remark 1* and we cannot obtain results for a greater time.

From the physical point of view, the main process now takes place in the film zone, whose area is negligibly small with respect to the area occupied by the bubble. So the global problem consists of two parts in this case: a small-scale film thinning process and a large-scale problem of the bubble motion. To describe the processes well we need to consider the first one with respect to its reference length, the film thickness $l_f \ll 1$, and the second with respect to the bubble diameter l. Perhaps the best way to study the next stage of the process is to use a film-thinning model for the film part and to couple it with our model for the bubble and the ambient liquid. This could be an interesting subject for further studies. On the other hand, the existing theories for the film stage seem to yield satisfactory results (see e.g. Reed *et al.* 1980). So it is not very obvious whether it is worth doing.

Therefore, it is clear that our theory describes the process of the bubble approach to a rigid wall up to the moment when the film thickness becomes comparatively small. In practice this moment is automatically indicated by the numerical method as previously described.

5.2. *Bubble approaching a rigid wall*

First we consider gas bubbles in two different real liquids – glycerin (figure 9) and aqueous sugar solution (figure 10). In the second case the gas and liquid are the same as those used by Bhaga & Weber (1981), see their figure 2(*b*). The only difference is that our results are obtained for a bubble with equivalent diameter twice as large as Bhaga & Weber.

The dimpling phenomenon is observed in both experiments for large times. A lubrication layer is formed between the wall and the gas–liquid interface. The viscous fluid is 'trapped' between the bubble and the rigid boundary and causes the dimpling, because the pressure drop is insufficient to overcome the viscous stress in

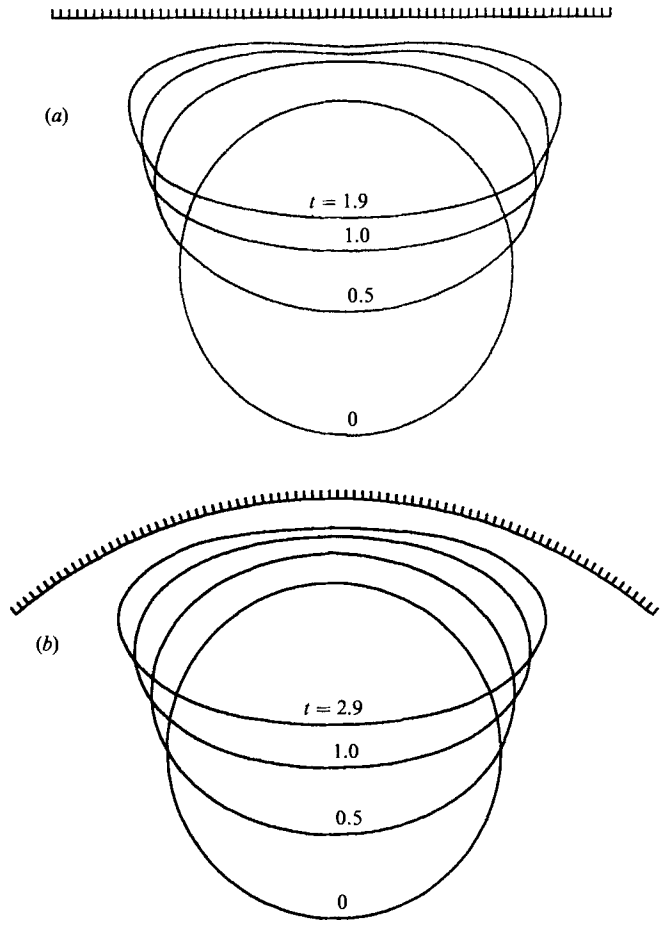

FIGURE 9. Time development of the shape of an air bubble with diametere 20 mm in glycerin, $\mathscr{R} = 0.396$, $\mathscr{E} = 19.48$, $\gamma = 0.75$: (*a*) $e = \infty$; (*b*) $e = 3$.

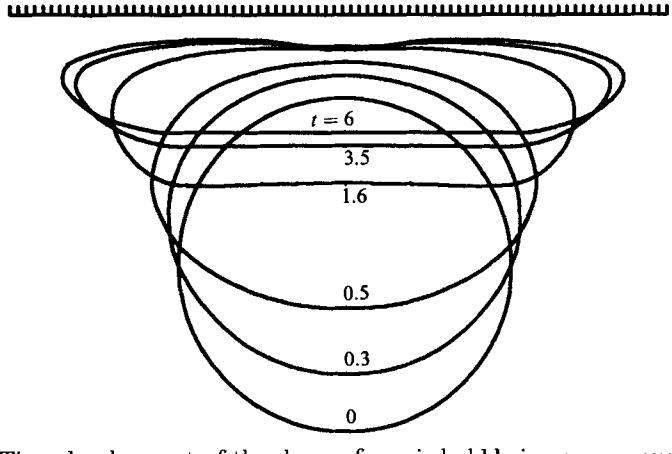

FIGURE 10. Time development of the shape of an air bubble in aqueous sugar solution at $\mathscr{R} = 1.24$, $\mathscr{E} = 70.8$, $\gamma = 0.75$.

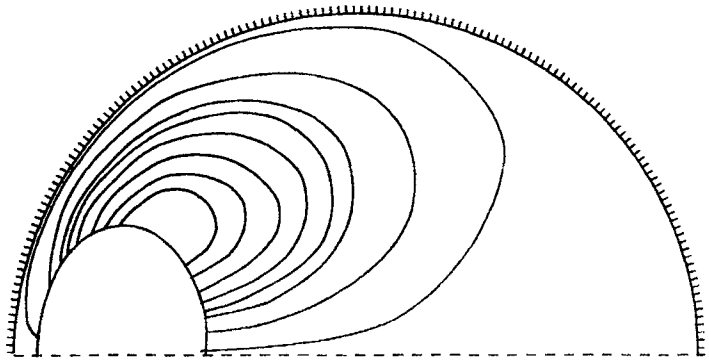

FIGURE 11. Instantaneous streamlines for a bubble approaching the container wall at $\mathscr{R} = 22.2$, $\mathscr{E} = 80$, $\gamma = 0.8$, $t = 0.18$.

the layer. This is evident on the axis in figures 9(*a*), 10, 12(*a*) and at a non-axial location in figure 13(*b*).

In figures 9, 12(*c*) and 13(*a*) the bubble velocity is seen to be smaller in the container (problem ii) than for the flow bounded by a plate (problem i) when the remaining conditions and governing parameters are the same. This is natural and is attributed to the influence of the container. For the same moment in time the thickness of the liquid layer that is formed between the bubble and the wall is larger for the flow in the container than for the case when the flow is bounded by a plate. This is no surprise since the non-slipping at the container wall results in a larger resistance to the outflow of the liquid from the near-wall zone than in the plate case $e = \infty$. In fact the hydrodynamical interaction of a deformable bubble with a container wall is stronger than with a plane wall.

The instantaneous pattern of the streamlines is presented in figure 11 and illustrates the outflow from the film zone and the rise of the bubble rear.

It is interesting to give a feeling for the influence of the four governing parameters on the properties of the scheme and algorithm as well as on the results obtained. In what follows this is done in detail through varying one of the parameters with the others being held fixed.

In figure 12 results are shown for the shape of a bubble rising towards a rigid wall (three governing parameters) for fixed Reynolds number $\mathscr{R} = 10$ and starting distance $\gamma = 0.75$ and different Eötvös numbers. It is interesting to note the occurrence of an indentation of the free surface at the rear of the bubble for comparatively large Eötvös number – figures 12(*c*) and 13(*a*). This effect is a consequence of the interplay between the inertia of the liquid behind the bubble and the deceleration of the particle's motion due to the presence of the wall. At the same moment the pressure maximum is located at the bubble rear. The liquid at the bubble rear is accelerated due to the particle's motion (under the buoyancy, in our case). It pushes the interface and penetrates into the particle, if the surface tension is not enough strong to stop it. This phenomenon could be referred as a jet formation, by analogy to a similar effect in a different problem – collapse of a vapour cavity near a plate, see Blake *et al.* (1986).

This effect is absent for comparatively small Reynolds and Eötvös numbers (figures 9 and 12*a*) and is evident for large ones (figures 13*a* and 15). Its amplitude is small for modest Reynolds and large Eötvös numbers (figures 10 and 12*c*) and in this case it could be considered as a bubble rear-flattening effect. In this connection

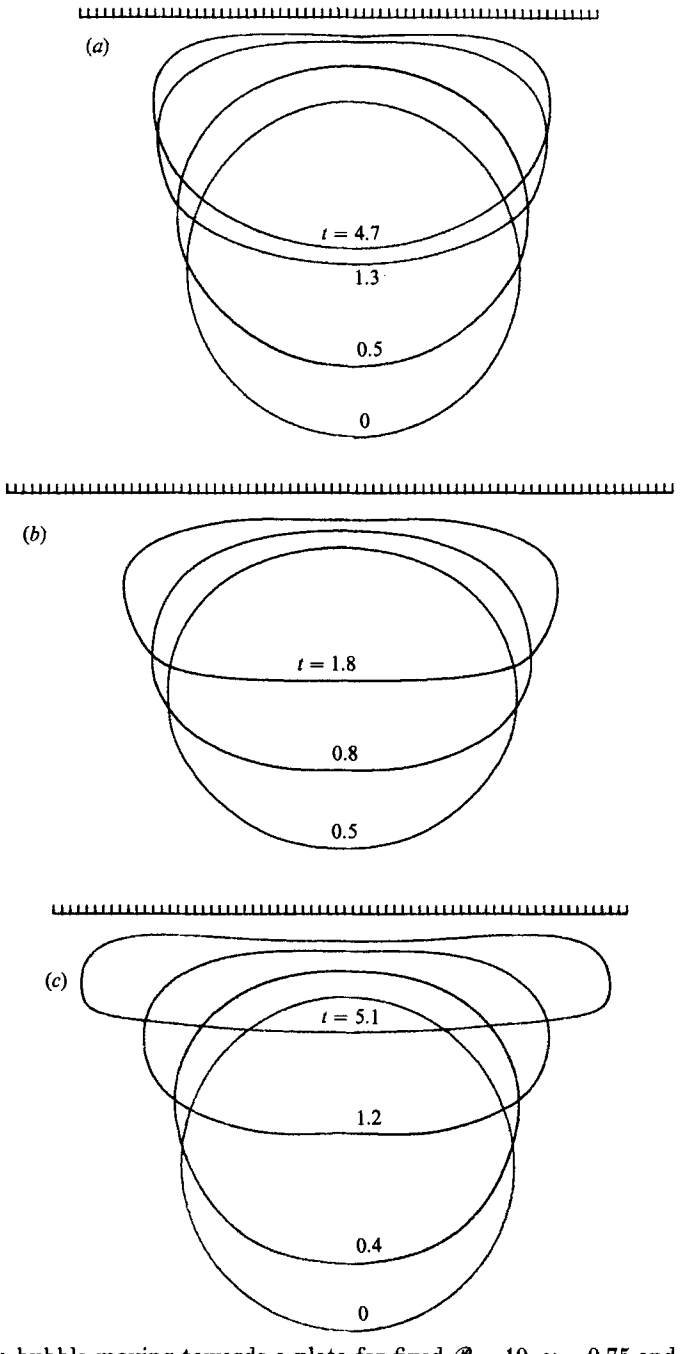

FIGURE 12. Gas bubble moving towards a plate for fixed $\mathscr{R} = 10$, $\gamma = 0.75$ and different values of the Eötvös number: (*a*) $\mathscr{E} = 7.2$; (*b*) $\mathscr{E} = 18$; (*c*) $\mathscr{E} = 36$.

we could mention that the curvature at the particle's rear diminishes in time for small Reynolds numbers (figure 9), but this is not so for larger ones (figure 12), although in both cases the indentation is absent.

Perhaps this jet could split the bubble if the surface tension and the viscosity were small and the particle's velocity were great at the moment of the start of the

interaction with the wall. But we have not observed it in our numerical calculations. Usually it causes a disturbance which disappears resulting in a surface wave – see figure 12(*b*). Sometimes the amplitude of the wave is very small and it is not visible in the numerical experiment (figures 10 and 13*a*).

A slight dimpling is observed in computations for $\mathscr{A} < 0.0875$. When $\mathscr{E}$ increases, the dimple exhibits a tendency to increase in amplitude and to occur further from the wall.

Many experimental and theoretical studies exist which treat the film-drainage and rupture problems (see Hodgson & Woods 1969; Burrill & Woods 1973; Jones & Wilson 1978). Chi & Leal (1989) classify film drainage into three general modes. In the first the film is thinnest at $r = 0$ and monotonically increases as r increases (so-called 'rapid' drainage). In the second the film thickness is considered as almost uniform. In the last case 'dimpled' drainage occurs, in which the film is thinnest at a rim of finite radius, rather than at $r = 0$. Film-drainage theories with zero tangential stress at the free boundaries predict minimum film thickness at the symmetry axis, while the theories with no-slip conditions predict 'dimpled' drainage. In the cases considered in this paper one of the film boundaries is immobile and the other is free. In almost all of our experiments the initial film profile is of the 'dimpled' type. Thus, the immobilization of even one of the film boundaries could cause the 'dimpled' drainage configuration. Geller *et al.* (1986) draw the same conclusions when investigating the motion of a rigid sphere towards a deformable fluid–fluid interface at low Reynolds numbers. As one can see below, an additional factor exists which influences the dimpling formation – the inertia of the fluid particle. This factor is not included in the available theoretical studies.

In order to reveal the influence of the container wall we repeat the above experiments but with $e = 3$. The general tendencies remain the same as in the above case $e = \infty$. No dimpling is observed for $\mathscr{E} = 7.2$ and 18. The thickness of the spherical thin liquid layer is almost constant. For the case $\mathscr{E} = 18$ an indentation in the rear part is observed for $t = 1.5$, and after that it disappears. The length r_f of the spherical thin liquid layer increases and its thickness in the middle becomes greater than that in the rims $r_f = 0.5625$, $\mathscr{A} = 0.0875$, $t = 2.9$.

In figure 13(*a*) the third numerical experiment from this series is depicted. A slight dimpling ring is observed at the film surface for $r = \pm 0.3125$. This is a zone where the curvature of the interface twice changes its sign. That also could be considered as an analogue of the 'classical' dimpling phenomenon in the case of a film between the bubble and spherical container. This phenomenon does not grow but fades away with time. A clear pattern of a toroidal dimpling is observed for large Eötvös number – see figure 13(*b*) – i.e. a dimple-ring is formed in the front part of the bubble not far from the rim. The effect is connected with the curvature of the wall and is due to the additional hydrostatic pressure gradient in the draining film because in this case the hydrostatic pressure grows in the radial direction and as a result the pressure maximum is moved from the central zone to the film edge. It is clearly observed in the numerical experiment that the velocity in the dimpling zone remains comparatively small with respect to the velocity near the front stagnation point. A similar effect was observed experimentally by Hartland (1968) for a spherical film on a rigid sphere.

Summing up our numerical results for the case of a curved wall, the film thickness will be greater at the line of symmetry than at the rim, which could be considered as a 'dimpling' drainage configuration in the case of a curved wall. The film drainage will again be slow. This phenomenon is not seen in figure 15 because the computations

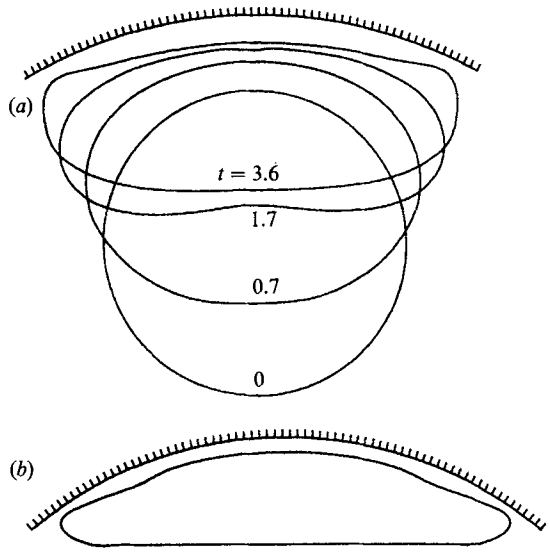

FIGURE 13. Gas bubble approaching the wall of a spherical container for $\gamma = 0.75$, $e = 3$: (*a*) $\mathscr{R} = 120$, $\mathscr{E} = 36$; (*b*) $\mathscr{R} = 1$, $\mathscr{E} = 360$.

are stopped at an early stage of the process but is clear in figure 13. Hence the presence of a curved rigid wall leads again to 'dimpling' drainage, as could be expected.

The phenomenon of ring dimpling is more special and occurs only for large curvature of the wall and deformability of the interface.

As expected the deformations h and w are more significant for larger Eötvös number. The tendency of the average deformation to grow with an increase of $\mathscr{E}$ and e is evident from figure 14.

In order to investigate the influence of the Reynolds number, numerical experiments are performed with fixed $\mathscr{E} = 18$. The first one for $\mathscr{R} = 10$ is shown on figure 12(*b*). The dimpling is not very well shown but the bubble has not yet achieved its 'terminal' shape. For $\mathscr{R} = 20$ the inertial effects (the concavity in the rear part and the receding of the ends of the film area from the wall) increases (not shown in the figures). Deformations become larger, but the length of the thin liquid layer zone does not change essentially. A clear dimpling is formed at the axis of symmetry which increases when the Reynolds number increases. This confirms the important role of the inertia of the particle in the dimple formation. These tendencies develop for $\mathscr{R} = 40$ and can be clearly observed in figure 15(*c*).

It is interesting to point out that for the case of a bubble in a container the general tendency remains the same as in the previous case $e = \infty$ (see figure 15*a*, *b*). The general rule that the bubble velocity in the container is smaller than near the plate again holds.

Taking the aspect ratio w/h as the sole measure for the deformation of the bubble it is interesting to investigate the dependence of this quantity on Reynolds number. The comparison between the aspect ratios obtained with different Reynolds numbers is depicted in figure 16. The deformation increases with $\mathscr{R}$ only for intermediate times and decreases for small ones. The non-monotonic behaviour of w/h as a function of $\mathscr{R}$ is an interesting feature of the results obtained. The explanation seems to be the following. From (2.5) is clear that for a given reference velocity large Reynolds

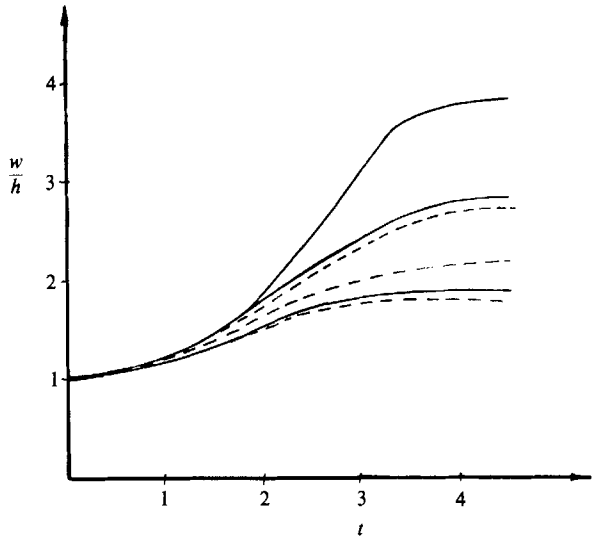

FIGURE 14. Comparisons of the average deformation w/h for fixed Reynolds number ($\mathscr{R} = 10$) and different Eötvös numbers ($\mathscr{E} = 7.2, 18, 36$), the higher line corresponds to larger $\mathscr{E}$, ——, $e = \infty$; – – –, $e = 3$.

numbers correspond to small driving forces. Hence it is natural to expect that for small times the bubble velocity decreases with the growth of $\mathscr{R}$, as observed in the numerical experiments depicted in figure 16.

It is interesting to mention here that for $\mathscr{R} = 20$ and $e = 3$ the bubble aspect ratio is greater than for $e = \infty$, which is an exception from the above-stated general rule. This is due to non-monotonic behaviour of w and is discussed in the end of this section.

The velocity of the bubble is a quantity that changes considerably with time for both problems under consideration. It rises from zero and then decays to nearly zero at the end of the simulation. Its maximum occurs for intermediate times when as a rule the reference velocity is attained. Hence the instantaneous Reynolds number $\mathbb{V}_{\max}(t)\mathscr{R}$ differs from $\mathscr{R}$, i.e. the standard Reynolds number does not characterize completely the hydrodynamics at each time moment.

The significant changes in bubble velocity seems to be the reason why the Weber number is not always a convenient parameter for describing the deformability of interface. If we use $\mathscr{R}$ and $\mathscr{W}$ as governing parameters the bubble deformations do not increase with the increase of $\mathscr{R}$ even for large times. The aspect ratio h/w is larger for $\mathscr{W} = 40$, $\mathscr{R} = 20$ than for $\mathscr{W} = 40$, $\mathscr{R} = 40$. Perhaps one might expect that $\mathscr{W}$ could have been a better choice for a governing parameter provided that another reference velocity is introduced, but it seems to us that this will not be the case.

In figure 17(*a*) bubble quasi-terminal shapes are depicted for different initial distances from the wall. The velocity at the moments under consideration is in the range of 10^{-3} (the bubble is moving very slowly) which allows us to assume that these are indeed the quasi-terminal shapes. At that time stage only the development of the dimpling at the front part is in progress.

It is observed in figure 17(*b*) that regardless of the value of starting distance the deformation characteristics w and h reach the same terminal values and after that remain nearly constant for large times. For small times the deformations exhibit more conspicuous dependence on the starting distance and are smaller for larger

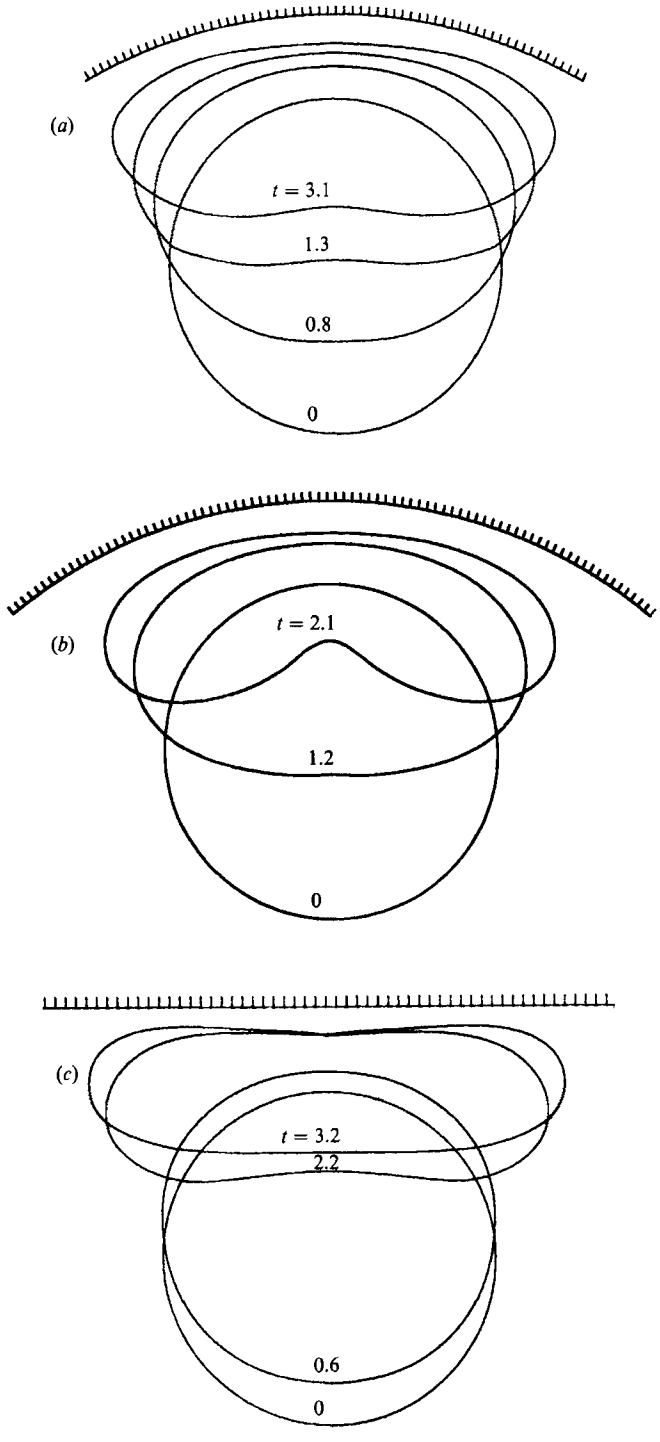

FIGURE 15. Gas bubble approaching a rigid wall for fixed $\mathscr{E} = 18$ and different Reynolds numbers: (*a*) $\mathscr{R} = 20$, $e = 3$; (*b*) $\mathscr{R} = 40$, $e = 3$; (*c*) $\mathscr{R} = 40$, $e = \infty$.

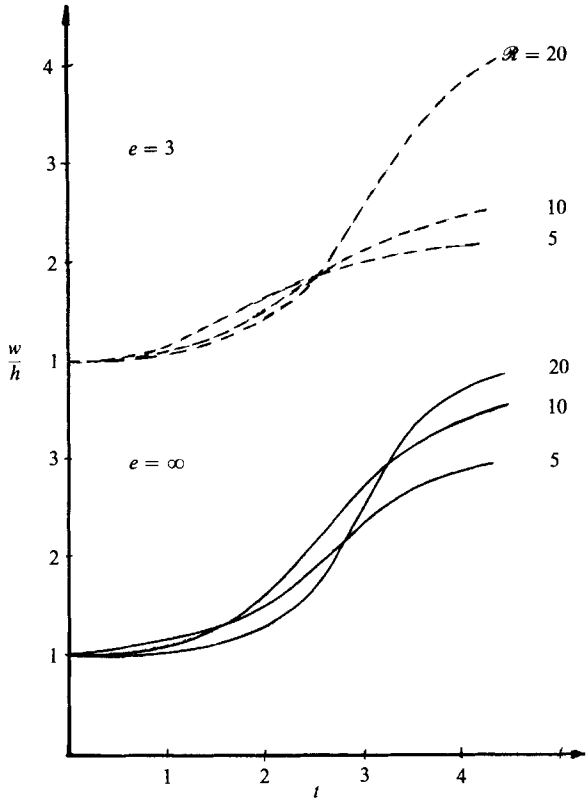

FIGURE 16. Comparison of the average deformation w/h for fixed $\mathscr{E} = 18$ and different $\mathscr{R}$.

starting distances owing to the weaker hydrodynamical interaction with the wall. Conversely, the greatest dimpling takes place for the starting distance $\gamma = 1$ (see figure 17*a*). Its depth is approximately 0.055, which is about 50% of the thickness of the bubble in the central zone. Dimpling is not observed at all for $\gamma \leqslant 0.55$, which supports the hypothesis that the dimpling phenomenon is connected with the specific value of the bubble velocity when the film is formed – see figure 17(*c*). The pressure maximum is now located near the centre of the dimpling zone where the velocity remains steadily lower than at the point where the film thickness is smallest – see figure 17(*d*).

The influence of the dimensionless container radius is also studied. As expected, the bubble height h decreases with decreasing e, see figure 18. It is clear that the presence of a spherical container wall opposes the 'flattening' of the bubble. But the behaviour of the dimensionless width w is non-monotonic. The greatest deformations in the radial direction occur for intermediate values of the wall curvature – see also figure 16. The explanation is that the front part of the interface follows the wall shape. For intermediate values of e a part of driving force is transformed through the hydrodynamical interaction with the wall to pull the rim zone in the radial direction. But this singularity is observed only for comparatively large Eötvös numbers.

It would be interesting to summarize and categorize the results in a chart similar to Bhaga & Weber (1981). But our problem depends on more parameters (on $\mathscr{R}$, $\mathscr{E}$, γ, e and t instead of $\mathscr{R}$ and $\mathscr{E}$) and we would need many experiments to do this really well. On the other hand it seems natural to think first about such a classification in

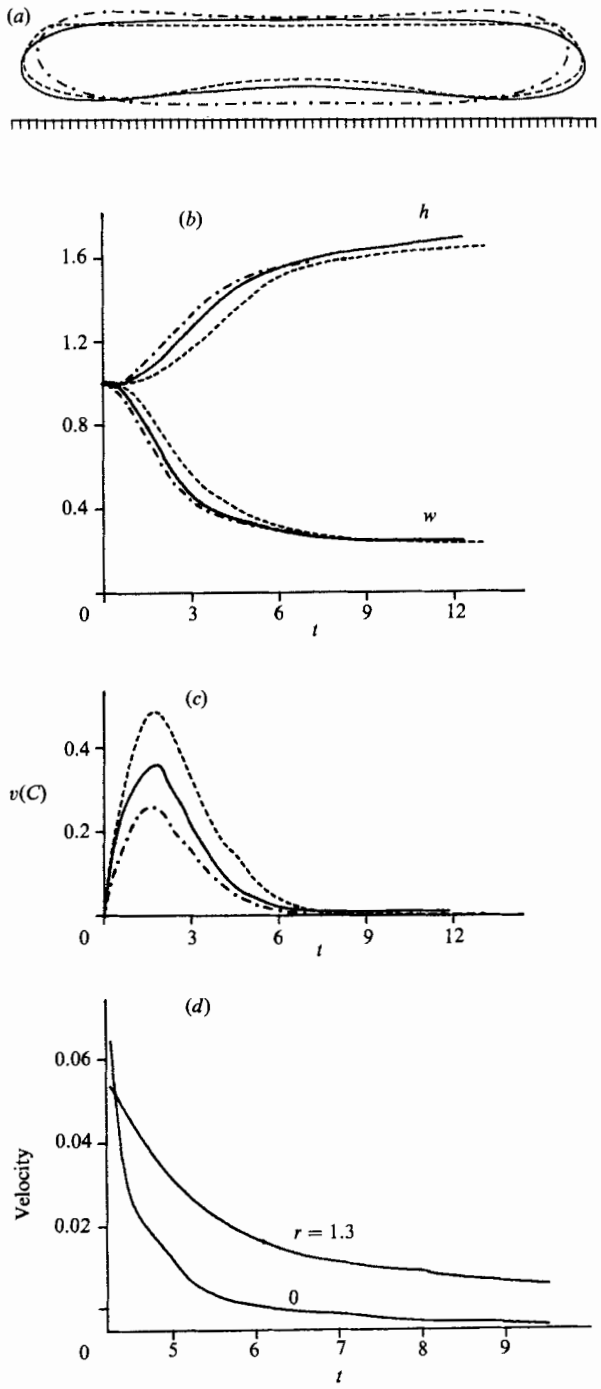

FIGURE 17. Comparison for different starting distances $\gamma = 1$ (– – –), $\gamma = 0.75$ (——) and $\gamma = 0.55$ (– · – · –) at $\mathscr{R} = 22.2, \mathscr{E} = 80$: (*a*) bubble terminal shapes; (*b*) bubble height h and width w; (*c*) bubble velocity $v(C)$; (*d*) the velocity at $r = 0$ and $r = 1.3$.

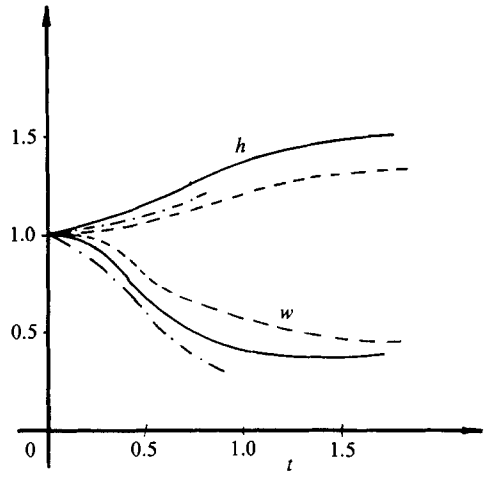

FIGURE 18. Comparison of w and h for different diameters of the container $e = 2$ (– – –), $e = 3$ (——) and $e = \infty$ (– · – · –) at $\mathscr{R} = 22.2$ and $\mathscr{E} = 80$.

the case of the unsteady motion of a bubble in unbounded liquid, i.e. for $\gamma = \infty$ and $e = \infty$.

5.3. *Bubble receding from a rigid wall*

The receding of the bubble from a rigid wall is a physical problem which differs from the one above considered. No films are formed and the influence of the wall is considerable only for relatively small time and small starting distances. In figure 19 the solution of problem (ii) is depicted for small starting distance, Reynolds and Eötvös numbers. The interface deformability is low and the viscous forces are large. The temporal evolution of the process is very slow. Considerable elongation of the bubble takes place near the wall. Again a lubrication layer is formed between the bubble rear and the rigid wall and it plays an important role in the process. The viscous force evidently dominates the gravitational one in this layer.

When the bubble reaches the central zone of the container it adopts a nearly spherical form again. This effect is due to the influence of the opposite wall and confirms the hypothesis stated by Brunn & Roden (1985).

The case of relatively large Reynolds number and intermediate Eötvös one is depicted in figure 20. For $t \leqslant 1.5$ the elongation effect is present but it is to a certain degree weaker than in the previous case. Clearly its amplitude diminishes with the growth of the Reynolds number. However, we could not say that this effect is absent in the inviscid case. Something similar was observed by Blake *et al.* (1986) (see their figure 5) in the rather different problem of a cavitation bubble collapsing near a wall in an ideal flow for large buoyancy influence and moderate time.

When the elongation of the bubble become sufficiently large the surface tension acts to round the bubble and after that the inertia forces come into play to preserve the somewhat higher speed of the liquid in the vicinity of the rear end, thus forming the concave shape in the rear part of the bubble. So the initial disturbance (elongation) cause an oscillation of the rear which develops into a surface wave. This wave is fading away in all numerical experiments. Perhaps if the initial disturbance were sufficiently great it could encompass the bubble and even lose stability. This effect is not observed for low Reynolds numbers.

In figure 20(*b*) the process development is shown for $\mathscr{R} = 120$ and $\mathscr{E} = 12$. The

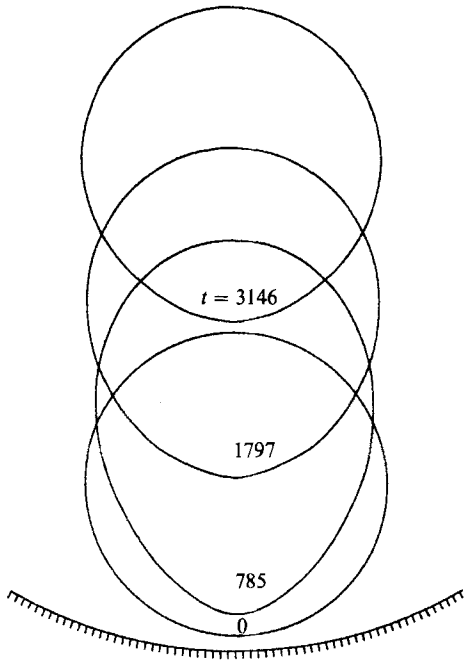

FIGURE 19. Bubble receding away from a rigid wall at $\mathscr{R} = 0.2$, $\mathscr{E} = 1$, $\gamma = 0.55$, $e = 3$.

tendencies mentioned for $e = \infty$ are observed here as well. The elongation of the rear end is now greater owing to the increase of the influence of the wall, and the concavity becomes even larger. Like the situation with the overall deformations, the magnitude of the depth for a given time is smaller for the case of spherical container than for the case of plane wall. This causes a wave with greater amplitude than in the case $e = \infty$.

6. Conclusions

The hydrodynamic behaviour of a bubble in the vicinity of a rigid plane wall is studied as well as the interaction of a bubble with the wall of a spherical container. The investigations are also applicable for drops if the viscosity of the liquid and pressure change in the drop are negligible.

A parametric investigation of these problems is done. The set of parameters includes the Reynolds number, the Eötvös number, the non-dimensional starting distance γ and the non-dimensional radius of the container e. The deformation increases when $\mathscr{R}$, $\mathscr{E}$ and e increase. Disappearance of the influence of γ for large time is observed.

Quantitative data for the occurrence and time development of the dimpling in the approaching case are obtained. We have computed bubble shapes up to quite large times. The velocities are rather small then, so the particle motion nearly stops with respect to the reference length. In this situation the bubble shape is nearly stable, as is the dimple. The behaviour of the shape of this dimple seems to be interesting in connection with film-thinning theory. The dimple depth increases with the growth of the Reynolds and Eötvös numbers, as well as of the starting distance. Its width grows with the increase of the Eötvös number.

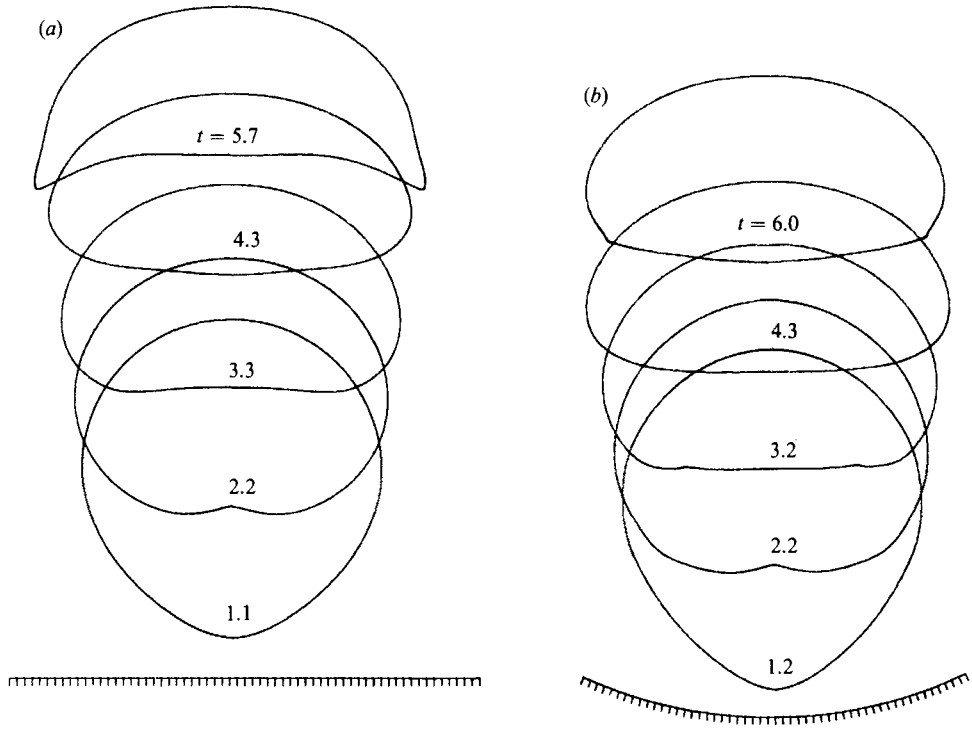

FIGURE 20. Bubble receding away from a rigid wall at $\mathscr{R} = 120$, $\mathscr{E} = 12$, $\gamma = 0.55$: (*a*) problem (i); (*b*) problem (ii).

Toroidal dimpling is observed when the bubble moves in a spherical container, a phenomenon not noticed by other authors.

The inertial effect concerning the appearance of a concavity in the rear part of the bubble is also observed. Its size increases when the Reynolds or the Eötvös number or the starting distance increases. This concavity is caused by the inertial forces in the liquid at the particle rear so this behaviour is to be expected. Perhaps if the inertia is great enough, it could disintegrate the bubble. If not, this disturbance disappears after a time and causes a surface wave at the interface. However, its amplitude is often small and this surface wave is not visible.

The receding of a bubble from a wall is considered, too. At first elongation of the bubble is observed. Its magnitude is connected with the value of the viscous forces in the gap between the particle and the wall. A lubrication layer is formed there, which plays an important role in determining the bubble shape. This elongation becomes larger with the growth of Eötvös number or the wall curvature and with the diminishing of the Reynolds number or the starting distance. Unfortunately we cannot be sure that this effect exists in the inviscid case: we can say only that if this were the case, the amplitude of the elongation will be smaller. When the particle has receded from the wall, the surface-tension forces begin to dominate the viscous ones at the bubble rear and this part of the interface begins to move to its equilibrium position. This causes a capillary wave on the surface of the bubble. If the damping influence of the viscous forces is not too great then it causes a concavity at the bubble rear, which fades away after a time.

A numerical method, and the package NEFIS based on it, for solving transient

problems of incompressible, viscous liquids are proposed. The numerical procedure belongs to the class of finite-element methods and is intended to solve the Navier–Stokes equations with gas–liquid or liquid–liquid boundaries. Test examples and comparisons with theoretical and experimental works of other authors are done, in the commonly used range of the governing parameters. They confirm the exactness of the results obtained.

Numerical experiments show that the method can predict complicated nonlinear effects such as dimple formation, concavity in the rear part of the bubble, capillary waves and so on.

Finally, the proposed method appears to be a useful tool for solving variety of similar problems with boundaries: of solid, gas–liquid or liquid–liquid type. The method can be also easily extended to treat liquid–liquid interfaces in the general case.

The authors are indebted to Professor R. Lazarov and Professor Ch. Christov for useful discussions as well as to the referees of the paper for their helpful comments.

REFERENCES

BATCHELOR, G. K. 1967 *An Introduction to Fluid Dynamics*. Cambridge University Press.

BAZHLEKOV, I., SHOPOV, P. & ZAPRYANOV, Z. 1989 Bubble motion in a rigid container. In *Proc. XIV National Summer School on Numerical Methods and Applications, Varna, Bulgaria, 1988*, pp. 182–201. Sofia: Publishing House of the Bulgarian Academy of Sciences.

BHAGA, D. & WEBER, M. E. 1981 Bubbles in viscous liquids: shapes, wakes and velocities. *J. Fluid Mech.* **105**, 61–85.

BLAKE, J. R., TAIB, B. B. & DOHERTY, G. 1986 Transient cavities near boundaries. Part 1. Rigid boundary. *J. Fluid Mech.* **170**, 479–497.

BLAKE, J. R., TAIB, B. B. & DOHERTY, G. 1987 Transient cavities near boundaries. Part 2. Free surface. *J. Fluid Mech.* **181**, 197–212.

BRADSTON, D. & KELLER, H. 1975 Viscous flow past spherical gas bubbles. *J. Fluid Mech.* **69**, 179–189.

BRUNN, P. O. & RODEN, T. 1985 On the deformation and drag of a type-A multiple drop at low Reynolds number. *J. Fluid Mech.* **160**, 211–234.

BURRILL, K. A. & WOODS, D. R. 1973 Film shapes for deformable drops at liquid–liquid interfaces. II. The mechanism of film drainage. *J. Colloid Interface Sci.* **42**, 15.

CHAO, B. T. 1969 Transient heat and mass transfer to a translating droplet. *Trans. ASME* C: *J. Heat Transfer*, May, 273–281.

CHERVENIVANOVA, E. & ZAPRYANOV, Z. 1985 On the deformation of two droplets in quasisteady Stokes flow. *Intl J. Multiphase Flow* **11**, 721–738.

CHERVENIVANOVA, E. & ZAPRYANOV, Z. 1987 On the deformation of a fluid particle moving radially inside a spherical container. *Phys.-Chem. Hydrodyn.* **8**, 293–305.

CHI, B. K. & LEAL, L. G. 1989 A theoretical study of the motion of a viscous drop toward a fluid interface at low Reynolds number. *J. Fluid Mech.* **201**, 123–146.

CHRISTOV, C. I. & VOLKOV, P. 1985 Numerical investigation of the steady viscous flow past a resting deformable bubble. *J. Fluid Mech.* **158**, 341–364.

CLIFFE, K. A. & LEVER, D. A. 1986 A comparison of finite-element methods for solving flow past a sphere. *J. Comput. Phys.* **62**, 321–330.

CLOUTMAN, L. D. 1987 A convective flux limiter for non-Lagrangian computational fluid dynamics. *J. Comput. Phys.* **73**, 349–363.

CONNOR, J. J. & BREBBIA, C. A. 1977 *Finite Element Techniques for Fluid Flow*. Newness Butterworths.

CUVELIER, C., SEGAL, A. & STEENHOVEN, A. A. VAN 1986 *Finite Element Methods and Navier–Stokes Equations*. D. Reidel.

DOMMERMUTH, D. G. & YUE, D. K. P. 1987 Numerical simulations of nonlinear axisymmetric flows with a free surface. *J. Fluid Mech.* **178**, 195–219.

EL SAWI, M. 1974 Distorted gas bubbles at large Reynolds number. *J. Fluid Mech.* **62**, 163–183.

FORTIN, A., FORTIN, M. & GERVAIS, J. J. 1987 A numerical simulation of the transition to turbulence in a two-dimensional flow. *J. Comput. Phys.* **70**, 295–310.

FREDERIKSEN, C. S. & WATTS, A. M. 1981 Finite-element method for time-dependent incompressible free-surface flow. *J. Comput. Phys.* **39**, 282–304.

GELLER, A. S., LEE, S. H. & LEAL, L. G. 1986 The creeping motion of a spherical particle normal to a deformable interface. *J. Fluid Mech.* **169**, 27–69.

GRESHO, P. M., LEE, R. L. & SANI, R. L. 1980 in *Recent Advances in Numerical Methods in Fluids* vol. A. Swansea: Pineridge.

HAPPEL, J. & BRENNER, H. 1965 Low Reynolds number Hydrodynamics. Prentice-Hall.

HARTLAND, S. 1967 The approach of liquid drop to a flat plate. *Chem. Engng Sci.* **22**, 1675–1687.

HARTLAND, S. 1968 The approach of a rigid sphere to a deformable liquid/liquid interface. *J. Colloid Sci.* **26**, 383–394.

HNAT, J. G. & BUCKMASTER, J. D. 1976 Spherical cap bubbles and skirt formation. *Phys. Fluids* **19**, 182–194.

HODGSON, T. D. & WOODS, D. R. 1969 The effect of surfactants on the coalescence of a drop at an interface. II. *J. Colloid Interface Sci.* **30**, 429.

JACKSON, C. P. 1987 A finite-element study of the onset of vortex shedding in flow past variously shaped bodies. *J. Fluid Mech.* **182**, 23–45.

JONES, A. F. & WILSON, S. D. R. 1978 The film drainage problem in droplet coalescence. *J. Fluid Mech.* **87**, 263–288.

KANG, I. S. & LEAL, L. G. 1987 Numerical solution of axisymmetric, unsteady free-boundary problems at finite Reynolds number. I. Finite-difference scheme and its application to the deformation of a bubble in a unaxial straining flow. *Phys. Fluids* **30**, 1929–1940.

KEUNINGS, R. 1986 An algorithm for the simulation of transient viscoelastic flows with free surface. *J. Comput. Phys.* **62**, 199–220.

LEVICH, B. 1949 Motion of gas bubbles at large Reynolds numbers. *Zh. Eksp. Teor. Fiz.* **19**.

MACKAY, G. D. & MASON, S. G. 1963 The gravity approach and coalescence of fluid drops at liquid interfaces. *Can. J. Chem. Engng* **41**, 203.

MIKSIS, M. J., VANDEN-BROECK, J. M. & KELLER, J. B. 1982 Rising bubbles. *J. Fluid Mech.* **123**, 31–41.

MINEV, P., SHOPOV, P. & ZAPRYANOV, Z. 1988 Numerical study of bubble's motion to or from a rigid wall. In *Proc. Conf. Numer. Methods and Applics.*, pp. 313–317. Sofia: Publishing House of the Bulgarian Academy of Sciences.

MOK, L. S. & KIM, K. 1987 Motion of a gas bubble inside a spherical liquid container with a vertical temperature gradient. *J. Fluid Mech.* **176**, 521–531.

MOORE, D. W. 1963 The boundary layer on a spherical gas bubble. *J. Fluid Mech.* **16**, 161–176.

PIRONNEAU, O. 1984 Recent development in the numerical solution of the Navier–Stokes equation. In *Analysis of Laminar Flow over a Backward Facing Step* (ed. K. Morgan, J. Periaux & F. Thomasset), pp. 21–31. Wiesbaden: Braunschweig.

REED, X. B., LEIDI, M. & HARTLAND, S. 1980 A two-dimensional model for the thinning of a planar film in narrow gap. *Phys. Chem. Hydrodyn.* **1**, 137–157.

RYSKIN, G. & LEAL, L. G. 1984 Numerical solution of free-boundary problems in fluid mechanics. Part 2. Buoyancy-driven motion of a gas bubble through a quiescent liquid. *J. Fluid Mech.* **148**, 19–35.

SHOKOOHI, F. & ELROD, H. G. 1987 Numerical investigation of the disintegration of liquid jets. *J. Comput. Phys.* **71**, 324–342.

SHOPOV, P. J. 1984 Condensation method for hydrodynamic problems. *Serdica* **10**, 198–205 (in Russian).

SHOPOV, P. J. 1985 Condensation method and its application for solving hydrodynamical problems, Ph. D. thesis (in Bulgarian), Bulgarian Academy of Science.

SHOPOV, P. J. 1988 Numerical method for free-surface hydrodynamical problems. *C. R. Acad. Bulg. Sci.* **41**, 37–41.

SHOPOV, P. J. 1989 Conservative properties of FEM for hydrodynamics. In *Proc. Conf. Numer. Methods and Applics., Sofia, August 22–27, 1988* (ed. Bl. Sendov *et al.*), pp. 449–453. Sofia: Publishing House of the Bulgarian Academy of Sciences.

SHOPOV, P. J. & MINEV, P. D. 1986 Numerical solution of viscous hydrodynamic problems with free boundaries. *University Ann. Appl. Maths* **22**, 211–220 (in Bulgarian).

SHOPOV, P. J., MINEV, P. D. & BAZHLEKOV, I. B. 1989*a* Grid redefinition and usage of splines in computer simulation of multiphase flows. In *Proc. XIV National Summer School on Numerical Methods and Applications, Varna, Bulgaria. 1988*, pp. 202–205. Sofia: Publishing House of the Bulgarian Academy of Sciences.

SHOPOV, P. J., MINEV, P. D. & BAZHLEKOV, I. B. 1990 Numerical method for unsteady viscous hydrodynamical problems with free boundaries. *Intl J. Numer. Meth. Fluids* (submitted).

SHOPOV, P., MINEV, P., BAZHLEKOV, I. & ZAPRYANOV, Z. 1989*b* Nonstationary motion of a deformable gas bubble in viscous liquid in the presence of wall. *C. R. Acad. Bulg. Sci.* **42**, 43–46.

TAYLOR, T. & ACRIVOS, A. 1964 On the deformation and drag of a falling viscous drop at low Reynolds number. *J. Fluid Mech.* **18**, 466–476.

THOMASSET, F. 1981 *Implementation of Finite Element Method for Navier–Stokes Equations*, Series in computational physics, Springer.